FILE

GUGGENHEIM JET PROPULSION CENTER
CALIFORNIA INSTITUTE OF TECHNOLOGY
PUBLICATION NO. 156

Reprinted from
Supersonic Flow, Chemical Processes and Radiative Transfer
PERGAMON PRESS
OXFORD . LONDON . EDINBURGH . NEW YORK . PARIS . FRANKFURT
1964

SIMILARITY PARAMETERS FOR RADIATIVE ENERGY TRANSFER IN ISOTHERMAL AND NON-ISOTHERMAL GAS MIXTURES*

S. S. PENNER†, M. THOMAS‡ and G. ADOMEIT§

Karman Laboratory of Fluid Mechanics and Jet Propulsion
Daniel and Florence Guggenheim Jet Propulsion Center
California Institute of Technology
Pasadena, California

SUMMARY

The similarity groups for multicomponent, reacting gas mixtures with radiative energy transport are derived (Section 1). The resulting relations are used to consider the feasibility of scaling for flow processes with radiative energy transport under highly simplified conditions (Sections 2 and 3). Next the scaling parameters are derived for radiant energy emission from isobaric and isothermal gases for arbitrary opacities and various spectral line and molecular band models (Section 4). Scaling parameters for radiant energy emission from isobaric but non-isothermal systems are discussed for arbitrary opacities and various spectral line and molecular band models under the restrictions imposed on the allowed temperature profiles for dispersion and Doppler lines by the Eddington–Barbier approximation (Section 5). Finally, we consider the radiative scaling properties for representative temperature profiles for both collision-broadened and Doppler-broadened line profiles on the basis of exact numerical calculations that we have performed for a rotational spectral line belonging to a molecular vibration–rotation band (Section 6). It appears that simple scaling rules generally constitute a fair approximation for dispersion lines in non-isothermal systems but that corresponding relations apply to lines with Doppler contour only in the transparent gas regime.

1. DETERMINATION OF SIMILARITY PARAMETERS

The techniques for identifying the similarity groups for systems described by a set of conservation equations are well known and have been developed in detail previously for reacting, multicomponent gas mixtures.[1] Although the particular form of the conservation equations used in the original

* Supported by the Air Force Office of Scientific Research under Contract AF49(638)-984.

† Professor of Jet Propulsion; currently on leave at the Institute for Defense Analyses, 1666 Connecticut Ave., N.W., Washington 9, D.C.

‡ Graduate Research Assistant, 1961–63.

§ NATO post-doctorate fellow, 1962–63; on leave from the Technische Hochschule, Aachen, Germany.

analysis has been shown to be in error in several respects,[2,3] the resulting similarity groups are unchanged if the same approximations are used as in the original article.[1] Some generalization of procedure can be made without difficulty by following the method described below (Eqs. (4) and (6) are not given in Ref. 1).

We start with the set of conservation equations (see Eqs. (12), (13), (16) to (18), and (23) in Chapter XVIII of Ref. 3); next we use a binary mixture approximation for each of the diffusion velocities (using Eq. (4) on p. 243 of Ref. 3, replace the subscript 1 by $K (K = 1, 2, \ldots n)$ for an n-component mixture, replace Y_2 by $1 - Y_K$ and W_2 by $\bar{W}'$ = average molecular weight of the fluid mixture remaining without species K); finally we write the complete heat flux vector (see Eq. (23) on p. 239 of Ref. 3) in the form[4]

$$q = -[\lambda + \lambda_{ch}]\nabla T$$

Here λ is the thermal conductivity associated with molecular collisions and λ_{ch} identifies the thermal conductivity associated with chemical reaction; λ_{ch} is given explicitly by the expression[4]

$$\lambda_{ch} = \sum_{K=1}^{n} \sum_{K'=1}^{n} \frac{(c)^2}{\rho} D_{KK'} W_{K'} H_K \frac{dX_{K'}}{dT}$$

where (c) = total number of moles per unit volume of mixture, ρ = fluid density, $D_{KK'}$ = multicomponent diffusion coefficient which is a known function of the binary diffusion coefficients and the mixture composition,[5] $W_{K'}$ = molecular weight of species K', H_K = molar enthalpy of species K, $X_{K'}$ = mole fraction of species K', T = temperature.

Using the specified starting relations and standard procedures,[1] we find the following set of similarity parameters for multicomponent, reacting gas mixtures without radiative energy transport if the subscript 0 identifies suitably chosen reference conditions:

γ_0 = ratio of specific heat at constant pressure ($\bar{c}_{p,0}$) to the specific heat at constant volume ($\bar{c}_{v,0}$) for the fluid mixture (1)

Reynolds numbers $\equiv Re_i = \rho_0 v_0 L_i/\mu_0$ (ρ = density, v = flow velocity, L_i = ith characteristic length, μ = mixture viscosity; $i = 1, 2, \ldots \xi$) (2)

Schmidt numbers $\equiv Sc_K = \mu_0/\rho_0 D_{K,0}$ ($D_{K,0}$ = diffusion coefficients for species K; $K = 1, 2, \ldots n$) (3)

$Sc_{K'} \equiv \mu_0/\rho_0 k_{TK,0} D_{K,0}$ (k_{TK} = thermal diffusion ratio for species K, $D_{TK,0} \equiv k_{TK,0} D_{K,0}$ = thermal diffusion coefficient for species K) (4)

Prandtl number $\equiv Pr = \bar{c}_{p,0}\mu_0/\lambda_0$ (5)

$Pr' \equiv \bar{c}_{p,0}\mu_0/\lambda_{ch,0}$ (this group will actually remain invariant if the groups Pr, Sc_K and $D_{\mathrm{III},i,r}$ are fixed) (6)

Mach number $\equiv M = \sqrt{(\rho_0 v_0^2/\gamma_0 p_0)}$ (p = pressure) (7)

Froude numbers $\equiv v_0^2/gL_i$ (g = gravitational acceleration) (8)

Damköhler's first similarity groups $\equiv D_{\mathrm{I},i,r} = L_i U_{r,0}/v_0$ ($U_{r,0}$ = characteristic reaction frequency for the rth chemical process; $r = 1, 2, \ldots m$), (9)

Damköhler's third similarity groups $\equiv D_{III,i,r} = q_r' U_{r,0} L_i / v_0 \bar{c}_{p,0} T_0$
(q_r' = heat release per unit mass in the rth chemical reaction) (10)
$\varphi = \frac{1}{2} v_0^2 / (\bar{c}_{p,0}/\gamma_0) T_0$. (11)

1.1 *Radiative Energy Transport in the Diffusion Approximation**

Throughout the following discussion we neglect photochemical reactions. In the diffusion approximation, the effective thermal conductivity is augmented by the term λ_{ra} where

$$\lambda_{ra} = 16\sigma T^3 / 3\bar{k}_{L,Ro}$$

σ = Stefan–Boltzmann constant and $\bar{k}_{L,Ro}$ = Rosseland mean absorption coefficient. Hence an additional analogue of the Prandtl number will appear, viz.

$$Pr^* = \bar{c}_{p,0}\,\mu_0 / \lambda_{ra,0} \tag{12}$$

In the momentum equation, an additional body force per unit volume

$$\mathbf{f}_{ra} = -(16\sigma T^3/3c)\nabla T$$

appears, where c = velocity of light. This body force per unit volume may be considered as an additive term to the pressure gradient, i.e. the fluid pressure is replaced by the sum of the fluid and radiation pressures. Thus a new similarity group may be formed which measures essentially the ratio of these pressures. It may be written as

$$\frac{16\sigma T_0^4}{3cp_0} = \frac{2}{3}\gamma_0 M^2 \frac{(4\sigma T_0^4/c)}{(\frac{1}{2}\rho_0 v_0^2)}$$

The ratio of the radiant energy density for a blackbody at the reference temperature $T_0 (= 4\sigma T_0^4/c)$ to the translational energy density under reference conditions ($= \rho_0 v_0^2/2$) we designate as the similarity group

$$\mathscr{R}_1 \equiv \frac{(4\sigma T_0^4/c)}{\rho_0 v_0^2/2} \tag{13}$$

The preceding considerations indicate that, in the diffusion approximation, allowance for radiative energy transfer leads to the requirement that an additional analogue to the Prandtl number (see Eq. (12)) and the similarity group $\mathscr{R}_1$ be considered. The reciprocal of the Rosseland mean absorption coefficient is the Rosseland mean free path $\bar{l}_{Ro}$ and is defined by the relation

$$\bar{l}_{Ro} = (\bar{k}_{L,Ro})^{-1} = \frac{15}{4\pi^4}\int_0^\infty \frac{1}{k_{L,\nu,T}} \frac{x^4 e^x}{(e^x - 1)^2}\,dx, \quad x = \frac{h\nu}{kT}$$

where $k_{L,\nu,T}$ identifies the linear absorption coefficient in the frequency interval between ν and $\nu + d\nu$ at the temperature T. Thus constancy of the similarity group Pr^* imposes severe restrictions on the allowed values of $k_{L,\nu,T}$ although it is not required that the products of the linear spectral

* For an elementary discussion of the basic equations, see Ref. 6.

absorption coefficients and characteristic lengths be maintained invariant as is necessary for radiative transfer problems for arbitrary opacities (see Section 1.3) in isothermal systems.

1.2. *Radiative Energy Transport for Transparent Gases*

The radiation pressure for transparent gases without external source is negligibly small. For isothermal systems, the energy loss from unit volume by radiation is[6]

$$\nabla \cdot \mathbf{F}_{ra} = 4\sigma T^4 \bar{k}_{L,Pl}$$

where $\bar{k}_{L,Pl}$ is the Planck mean absorption coefficient which equals the spectral emissivity per unit length. The term $\nabla \cdot \mathbf{F}_{ra}$ occurs as an additional term to the internal energy flow rate per unit volume

$$\rho \mathbf{v} \cdot \nabla u$$

where u represents the specific internal energy. Hence we may construct the ratio

$$\frac{4\sigma T^4 \bar{k}_{L,Pl}}{\rho \mathbf{v} \cdot \nabla u} = 4\gamma_0 \left(\frac{\sigma T_0^4 \bar{k}_{L,Pl,0} L_i}{\rho_0 v_0 \bar{c}_{p,0} T_0} \right) \left[\frac{(T^*)^4 \bar{k}_{L,Pl}{}^*}{\rho^* \mathbf{v}^* \cdot \nabla u^*} \right]$$

where the starred quantities are dimensionless. The parameters

$$\Gamma_i \equiv \frac{\sigma T_0^4 \bar{k}_{L,Pl,0} L_i}{\rho_0 v_0 \bar{c}_{p,0} T_0} \tag{14}$$

measure the ratio of radiative energy loss from the system per unit surface area to the free stream rate of enthalpy transport per unit area. The parameter Γ_i plays an important role in problems on stellar turbulence.[7]

Other important similarity groups in flows with radiant energy transfer are the Bouguer numbers

$$Bu_{\nu,i} \equiv k_{L,\nu,T,0} L_i \tag{15}$$

or

$$Bu_{Pl,i} = \bar{k}_{L,Pl,0} L_i \tag{15a}$$

or

$$Bu_{Ro,i} = \bar{k}_{L,Ro} L_i \tag{15b}$$

and the Boltzmann number

$$Bo = \frac{\sigma T_0^3}{\rho_0 v_0 \bar{c}_{p,0}} \tag{16}$$

The Boltzmann number is seen to arise from the similarity group Γ_i by dividing this quantity by the ith Bouguer number $Bu_{Pl,i}$.

1.3. *Radiative Energy Transport for Arbitrary Opacities**

When neither the diffusion approximation nor the transparent gas approximation are applicable, proper allowance for radiative energy

* This important problem is considered in detail in Section 4 for isothermal emitters and in Section 5 for non-isothermal systems.

transport becomes particularly difficult since *local* radiant energy contributions are determined by *integrals* over the accessible field of view. Neglecting photochemical processes, it appears now that complete simulation is possible, even for isothermal systems, only if a set of similarity groups involving the parameters $Bu_{\nu,i}$ remains invariant for all important lengths L_i at all frequencies ν. For non-isothermal systems, the problem becomes complicated still further because simulation now requires invariance of similarity groups involving the spectral radiant flux per unit solid angle at $\mathbf{x}_1$ with the solid angle measured (see Fig. 1) in the direction $(\mathbf{x}_2 - \mathbf{x}_1)/|\mathbf{x}_2 - \mathbf{x}_1|$, i.e. along C, viz.

$$\frac{1}{\pi}\int_{\mathbf{x}_{1,C}}^{\infty} [R_\nu^0(\mathbf{x}_2)][k_{L,\nu,T}(\mathbf{x}_2)] \left\{ \exp - \int_{\mathbf{x}_{2,C}}^{\mathbf{x}_{1,C}} [k_{L,\nu,T}(\mathbf{x})]\, dx \right\} dx_2$$

where the symbol C indicates that integration is to be performed along the path defined by a straight line drawn between the ends of (initially chosen) vectors $\mathbf{x}_2$ and $\mathbf{x}_1$. Here the scalar spectral blackbody radiancy $R_{\nu,0}^0$ and the scalar linear spectral absorption coefficients are, in general, complicated functions of the spacial location.

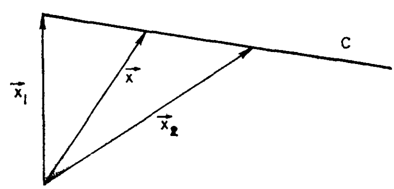

Fig. 1. Schematic diagram showing the definitions of $\mathbf{x}_1$, $\mathbf{x}$, $\mathbf{x}_2$ *and* C.

2. SCALING OF FLOW WITH MAINTENANCE OF CONSTANT VALUES OF $D_{I,i,r}$ AND Γ_i FOR TRANSPARENT GASES

An interesting special case, which is of some practical importance, involves the scaling of reactive gas flows for a given chemical system in such a way that the reference temperature, velocity and specific heats are invariant.

Let us identify by the subscripts H and Mo a large-scale burner and the model, respectively. It follows then from Eqs. (9) and (14) that

$$\frac{L_{i;H} U_{r,0;H}}{v_{0;H}} = \frac{L_{i;Mo} U_{r,0;Mo}}{v_{0;Mo}}$$

and

$$\frac{\sigma T_{0;H}^3 \bar{k}_{L,Pl,0;H} L_{i;H}}{\rho_{0;H} v_{0;H} \bar{c}_{p,0;H}} = \frac{\sigma T_{0;Mo}^3 \bar{k}_{L,Pl,0;Mo} L_{i;Mo}}{\rho_{0;Mo} v_{0;Mo} \bar{c}_{p,0;Mo}}$$

Let

$$n_\eta = \frac{\eta_{0;H}}{\eta_{0;Mo}} \tag{17}$$

denote the scaling parameter for the physical variable η. Furthermore, let us consider two propellant streams that are injected at the same reference conditions with

$$n_v = n_{c_p} = n_T = 1$$

The specified requirements for similarity now reduce to the relations

$$n_{L_i} n_{U_r} = 1 \tag{18}$$

and

$$n_{\bar{k}_{L,Pl}} n_{L_i} = n_\rho \tag{19}$$

Since

$$n_{U_r} \propto n_\rho^{o_r - 1} \tag{20}$$

if o_r represents the overall order of the rth chemical process, we may rewrite Eq. (18) in the form

$$n_{L_i} = n_\rho^{1 - o_r} \tag{21}$$

Therefore, the similarity groups $D_{\mathrm{I},i,r}$ will remain invariant if model tests are performed on small-scale engines at elevated density since o_r will generally be larger than unity. For example, for second-order processes ($o_r = 2$), $n_{L_i} = 10$ if the model tests are performed on a scaled-down burner in which all lengths have been reduced by a factor of 10. At the same time, $n_\rho{}^{1-o_r} = n_\rho{}^{-1} = 10$ if $n_\rho = 10^{-1}$, i.e. model tests should be carried out at densities ten times larger than those which are of interest for the full-scale device.

Combining Eqs. (19) and (21) we find that

$$n_{\bar{k}_{L,Pl}} = n_\rho^{o_r}$$

whence it follows that simultaneous similarity with respect to the groups $D_{\mathrm{I},i,r}$ and Γ_i can be maintained only for first-order processes since we expect, in general, that $n_{\bar{k}_{L,Pl}} \propto n_\rho$. To summarize, it is not possible to maintain simultaneously similarity in model tests and in large-scale burners with respect to the important similarity groups $D_{\mathrm{I},i,r}$ and Γ_i except in the unrealistic case that the effective, overall reaction order is unity.

3. SCALING OF FLOW WITH MAINTENANCE OF CONSTANT VALUES OF $D_{\mathrm{I},i,r}$ AND $Bu_{Pl,i}$ FOR TRANSPARENT GASES

The scaling procedures discussed in the preceding Section 2 were designed to assure similarity of chemical reaction profiles and of radiative energy loss rate per unit area relative to the convective energy transport rate per unit area. Thus they were designed to maintain the flow field in a reacting system invariant under the influence of radiant energy loss.

For some applications it may be more important to require invariance of the chemical composition profile and of the absolute value of the radiant energy emission rate per unit area of reaction front since the occurrence of radiant energy loss generally constitutes only a small perturbation on the flow field. In this case, it is pertinent to demand invariance of the Bouguer numbers $Bu_{Pl,i}$ as well as of $D_{\mathrm{I},i,r}$.

In order to assure invariance of $Bu_{Pl,i}$ we impose the condition

$$\bar{k}_{L,Pl,0;H}L_{i;H} = \bar{k}_{L,Pl,0;Mo}L_{i;Mo}$$

or

$$n_{\bar{k}_{L,Pl}}n_{L_i} = 1 \tag{22}$$

Equations (18) and (21) apply as before for $n_v = 1$. If we combine Eqs. (21) and (22) we obtain the result

$$n_{\bar{k}_{L,Pl}} = n_\rho^{o_r - 1}$$

i.e. the condition

$$n_{\bar{k}_{L,Pl}} = n_\rho$$

is now only satisfied for effective, overall, second-order processes. To summarize, simultaneous invariance of the similarity groups $D_{\mathrm{I},i,r}$ and $Bu_{Pl,i}$ is possible only for the important case of second-order, overall rate processes. For this case, the groups Re_i and M are also maintained invariant for a given combustible mixture.

The foregoing considerations lead to the important conclusion that significant model testing of the radiative properties of reacting gas flows is possible for those cases in which radiant energy emission does not produce significant perturbations in the flow field (e.g. transparent gases) provided we are satisfied in scaling the radiative properties per unit area of reacting mixture. The correlated changes in geometrical specifications (L_i) and operating density (ρ) are determined through Eq. (21) for $n_v = n_{c_p} = n_T = 1$.

4. SCALING PARAMETERS FOR RADIANT ENERGY EMISSION FROM ISOBARIC AND ISOTHERMAL SYSTEMS FOR ARBITRARY OPACITIES AND VARIOUS SPECTRAL LINE AND MOLECULAR BAND MODELS

For isothermal systems at the temperature T, the emitted steradiancy may be calculated from the equation

$$B(T) = \frac{1}{\pi}\int R_\omega^0 \left[1 - \exp\left(-P_\omega X\right)\right] d\omega$$

The results of these calculations are summarized in Table 1a for selected spectral line shapes and in Table 1b for selected vibration–rotation band models.

From the data listed in Tables 1a and 1b, we may draw the following important conclusions:

1. For transparent gases, the steradiancy is directly proportional to ρL irrespective of the spectral line contour or of the band model.
2. The important scaling parameter is ρL at all optical depths for isolated Doppler-broadened lines, and for all band models in which the spectral line structure is effectively smeared out.
3. The steradiancy is proportional to $\sqrt{(\rho^2 L)}$ at moderate to large optical depths (a) for isolated, collision-broadened lines, (b) for isolated lines with combined collision and Doppler broadening falling in the " square-root region " of the curves of growth. Also, for statistical distributions of the lines described under (a) and (b), $\sqrt{(\rho^2 L)}$ is the important scaling parameter.

Table 1a. Radiation Scaling Rules for Selected Line Shapes, Isothermal Emitters

Assumed Line Contour	*Function of Density (ρ) and Geometrical Length (L) which Assures Constancy of the Line Radiancy*	*Restrictive Conditions*	*Basic Equation(s) or Figures*
Pure natural line-broadening	ρL^* $\sqrt{(\rho L)}^*$	$(SX/2\pi b) < (2/\pi)$ $(SX/2\pi b) > (2/\pi)$	Eq. (4–28) Eq. (4–29) for constant b
Pure collision-broadening	ρL^* $\sqrt{(\rho^2 L)}^*$	$(SX/2\pi b) < (2/\pi)$ $(SX/2\pi b) > (2/\pi)$	Eq. (4–28) Eq. (4–29) for $b \propto p$
Pure Doppler-broadening	ρL^* ρL $\sqrt{[\ln (P'X)]}^* = \sqrt{[\ln (P'R_g T\rho L)]}^*$	$P'X \ll 1$ none $\ln (P'X) \gg 1$	Eq. (4–8) Eq. (4–10), (4–11)
Combined Doppler- and collision-broadening	ρL^* $\sqrt{(\rho^2 L)}^*$	$P_\omega X \ll 1$ for all ω " square-root region " of the curves of growth where $P'X$ is sufficiently large to make R_L independent of the line contour near the line center for all values of a	Eq. (4–35) Fig. 4–6
First-order Stark-broadening	$\rho L n_e^*$	$P_\omega X \ll 1$ for all ω	Eqs. (3–48), (3–48a)

Notes:

(*a*) Quantities identified with an asterisk indicate that the line radiancy is directly proportional to the specified function of ρ and L; without asterisk, constancy of the line radiancy is determined by the specified function of ρ and L although no simple proportionality exists.

(*b*) Equation and figure numbers refer to the book *Quantitative Molecular Spectroscopy and Gas Emissivities* by S. S. Penner, Addison-Wesley, Reading, Mass., 1959.

(*c*) P_ω = spectral absorption coefficient at the wave number ω (in cm^{-1}–atm^{-1}); X = optical depth (in cm–atm); S = integrated absorption of a spectral line (in cm^{-2}–atm^{-1}); b = dispersion semi-half-width of a spectral line (in cm^{-1}); P' = maximum value of the spectral absorption coefficient at the line center for a spectral line with pure Doppler-broadening; n_e = number of electrons per unit volume.

Table 1b. Radiation Scaling Rules for Selected Vibration-Rotation Band Models, Isothermal Emitters

Assumed Band Model	*Function of Density (ρ) and Geometrical Length (L) which Assures Constancy of the Band Radiancy*	*Restrictive Conditions*	*Basic Equation(s)*
Non-overlapping spectral lines	Applicable results for isolated spectral lines (see Table 1a)	The assumed line contour applies for all of the spectral lines which determine the total band radiancy	Applicable equations as listed in Table 1a
Rectangular box model	ρL^* ρL	$(\alpha X/\Delta\omega) \ll 1$ none	Eqs. (11–25), (11–26) Eqs. (11–25), (11–26)
Just overlapping line model	ρL^* ρL $\sqrt{[\ln (C\alpha X/\Delta\omega)]^*}$, C = Euler's constant	$P_\omega X \ll 1$ for all ω none $(\alpha X/\Delta\omega) \to \infty$, rotational fine structure smeared out	Eq. (11–50) Eq. (11–49) Eq. (11–143) *et seq.*
Statistical distribution of collision-broadened lines	ρL^* ρL $\sqrt{(\rho^2 L)}$	$(\bar{S}X/2\pi b) \ll 1$ and $(\bar{S}X/\delta^*) \ll 1$ $(\bar{S}X/2\pi b) \ll 1$ $(\bar{S}X/2\pi b) \gg 1$	Eq. (11–120a) Eq. (11–120a) Eq. (11–120b)
Statistical distribution of Doppler-broadened lines	ρL^* ρL	$P_\omega X \ll 1$ for all ω; $(\bar{S}X/\delta^*) \ll 1$ none	Eqs. (11–118), (4–8) Eqs. (11–118), (4–8)
Statistical distribution of spectral lines with combined Doppler- and collision-broadening	ρL^* $\sqrt{(\rho^2 L)}$	$P'X \ll 1$ and $\bar{S}X/\delta^* \ll 1$ square-root region of the curves of growth for all important contributing spectral lines	Eq. (11–118) and Fig. 4–6 Eq. (11–118) and Fig. 4–6
All other band models	ρL^*	$P_\omega X \ll 1$ for all ω	

Notes:

(*a*) Quantities identified with an asterisk indicate that the band radiancy is directly proportional to the specified function of ρ and L; without asterisk, constancy of the band radiancy is determined by the specified function of ρ and L although no simple proportionality exists.

(*b*) Equation and figure numbers refer to the book *Quantitative Molecular Spectroscopy and Gas Emissivities* by S. S. Penner, Addison-Wesley, Reading, Mass., 1959.

(*c*) P_ω = spectral absorption coefficient at the wave number ω (in cm^{-1}–atm^{-1});
α = integrated absorption of a vibration-rotation band (in cm^{-2}–atm^{-1});
$\bar{S}$ = constant value of the integrated absorption for each of the spectral lines contributing to the statistical distribution (in cm^{-2}–atm^{-1});
P' = maximum value of P_ω at the line center for a spectral line with pure Doppler-broadening.
X = optical depth (in cm–atm);
$\Delta\omega$ = effective width of a vibration-rotation band (in cm^{-1});
b = dispersion semi-half-width of the spectral lines (in cm^{-1});
δ^* = mean spacing of spectral lines (in cm^{-1});

5. SCALING PARAMETERS FOR RADIANT ENERGY EMISSION FROM ISOBARIC BUT NON-ISOTHERMAL SYSTEMS FOR ARBITRARY OPACITIES AND VARIOUS SPECTRAL LINE AND MOLECULAR BAND MODELS

One of the classical approaches to the theoretical calculation of radiant energy emission from non-isothermal systems is exemplified by the Lundblad series development for the solar photosphere.[7]

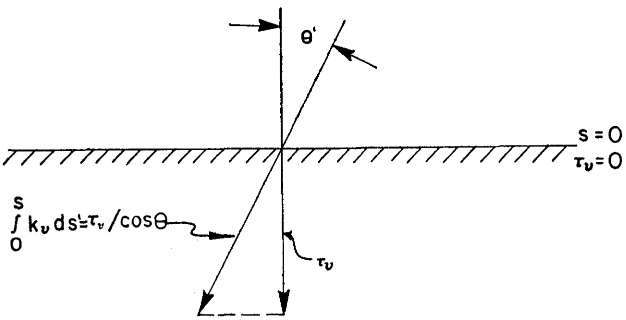

Fig. 2. Schematic diagram showing the geometric configuration discussed in the text.

The spectral steradiancy at the frequency ν and at the optical depth $\tau_\nu = 0$, corresponding to the geometrical length $s = 0$, in the direction θ' (see Fig. 2), is given by the relation

$$B_\nu(0,\theta') = \int_0^\infty B_\nu^0(\tau_\nu)\ \{\exp[-\tau_\nu \sec\theta']\}\ (\sec\theta')\ d\tau_\nu$$

$$= \int_0^\infty B_\nu^0(s) \left\{ \exp\left[- \int_0^s k_{L,\nu}(s')\ ds' \right] \right\} k_{L,\nu}(s)\ ds \tag{23}$$

where B_ν^0 is the blackbody steradiancy for local thermodynamic equilibrium at the optical depth

$$\tau_\nu = \cos\theta' \int_0^s k_{L,\nu}(s')\ ds'$$

corresponding to the geometric length s, along the beam of the emitting system, for a spectral linear absorption coefficient $k_\nu \equiv k_{L,\nu}$.

If $B_\nu^0(\tau_\nu)$ is developed in a (Lundblad) power series in τ_ν, viz.

$$B_\nu^0\ (\tau_\nu) = \sum_{i=0}^\infty a_i \tau_\nu^i \tag{24}$$

then

$$B_\nu(0,\theta') = \sum_0^\infty a_i \cos^i\theta' \int_0^\infty y^i\, e^{-y}\, dy = \sum_0^\infty a_i i!\, \cos^i\theta' \tag{25}$$

where the substitution $y = \tau_\nu \sec \theta'$ has been used. Comparison of Eqs. (24) and (25) shows that

$$B_\nu(0,\theta') = B_\nu^0(T_{\tau_\nu = \cos\theta'}) \text{ for } a_i = 0 \text{ if } i \geqq 2 \tag{26}$$

i.e. if only the first two terms are used (Eddington–Barbier approximation) in the power series given in Eq. (24). The physical interpretation of Eq. (26) is the following: the spectral steradiancy at $\tau_\nu = 0$, observed at an angle θ', for a non-isothermal system is identically equal to the numerical value of the spectral blackbody steradiancy $B_\nu^0(T_{\tau_\nu = \cos\theta'})$ at the optical depth $\tau_\nu = \cos\theta'$ or at the geometrical length defined by

$$\int_0^s k_{L,\nu}\, ds' = 1,\text{*}$$

provided only two terms are used in the power series expansion shown in Eq. (24).

It is interesting to consider the possible temperature profiles for selected spectral line shapes that are consistent with the statements

$$\begin{aligned} B_\nu^0(\tau_\nu) &= a_0 + a_1\tau_\nu = a_0 + a_1 \cos\theta' \int_0^s k_\nu(s')\, ds' \\ &= B_\nu^0(0) + [B_\nu^0(T_{\tau_\nu = \cos\theta'}) - B_\nu^0(0)] \int_0^s k_\nu(s')\, ds' \end{aligned} \tag{27}$$

and

$$\int_0^s k_\nu(s')\, ds' = 1 \tag{28}$$

We assume a monotone variation of T and τ_ν with s (and thus also of τ_ν with T) and we impose the boundary condition $T = T_0$ at $\tau_\nu = s = 0$. Differentiation of Eq. (27) with respect to T yields the differential equation

$$(\cos\theta')\, k_\nu(T) \frac{ds}{dT} = \frac{1}{a_1} \frac{dB_\nu^0}{dT} = \frac{1}{a_1} \frac{2h^2\nu^4}{c^2} \frac{1}{kT^2} \frac{\exp(h\nu/kT)}{[\exp(h\nu/kT) - 1]^2} \tag{29}$$

It is now possible to specify $k_\nu(T)$ for various spectral line profiles belonging to various assumed atomic or molecular emitters. We may then integrate Eq. (29) in order to find s as a function of T. Finally, Eq. (28) may be used to obtain the proper value of s, and hence of T, for which

$$B_\nu(0, \theta') = B_\nu^0\left(T \text{ for } \int_0^s k_\nu(s')\, ds' = 1\right).$$

In the analysis presented in Eqs. (23)–(29), it has been assumed that the quantities a_1 are constants. For an emitting system with structure, this

* Note that s is measured along the direction θ' shown in Fig. 2.

statement can be true only spectrally, i.e. a different value of a_1 must be chosen at a different frequency *for any specified temperature dependence on geometrical length.* The implications of this fact may be clarified by referring to the schematic diagram shown in Fig. 3. The temperature profile must, of course, be independent of frequency in any physically meaningful problem. However, the physical location s and the temperature T at which Eq. (28) is satisfied are strongly dependent on frequency. In the near line wing at the frequency $\nu_0 + \Delta\nu_1$, the integral condition of Eq. (28) will be met for small values of s and T; on the other hand, in the far wings of spectral lines where $\nu = \nu_0 + \Delta\nu_2$, much larger values of s, and hence of T, are required (compare Fig. 3). In other words, the contributions to $B_\nu(0, \theta')$

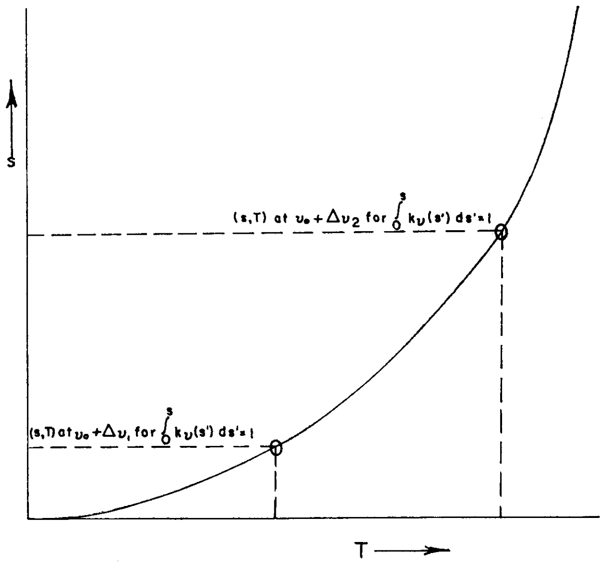

Fig. 3. *Schematic diagram showing the relation between temperature T and distance s for a specified angle θ'. The values of s and T required to satisfy Eq.* (28) *are shown for the representative frequencies $\nu_0 + \Delta\nu_1$ in the near wing and $\nu_0 + \Delta\nu_2$ in the far wing of a line.*

calculated according to Eq. (26) arise from regions of different temperature at different locations for different frequencies in such a way that the far line wings will make relatively larger contributions since they may be " seen " at greater geometrical depths and, correspondingly, at higher temperatures.

Since a_1 may vary with frequency, it will prove to be convenient to introduce a frequency dependence for a_1 deliberately in such a way as to allow a universal representation of a reduced distance variable (which is a function of ν) as a function of T.

5.1. *Isolated Spectral Lines Belonging to Diatomic Emitters with Collision-Broadening*

For local thermodynamic equilibrium, we find for diatomic emitters, to the harmonic-oscillator and rigid-rotator approximation, the following relation for collision broadening:

$$k_\nu = \frac{c^2}{8\pi^2\nu_0^2} A_{u\to l}\, g_u \left(\frac{p}{kT_0}\right) \frac{\sigma_0}{b_0} \left(\frac{T_0}{T}\right)^{3/2} [1 - \exp(-u_0 T_0/T)] \times$$
$$\times [1 - \exp(-h\nu_0/kT)] \times$$
$$\times [\exp(-E_l/kT)]\{1 + [(\nu - \nu_0)^2/(b_0^2 T_0/T)]\}^{-1} \qquad (30)$$

Here ν_0 is the frequency at the center of the emitted spectral line; $A_{u\to l}$ is the Einstein coefficient for spontaneous emission for the transition producing the given spectral line; g_u is the statistical weight of the upper energy level involved in the transition; p/kT_0 represents the number of molecules per unit volume at the pressure p and at the reference temperature T_0 with k denoting the Boltzmann constant; $\sigma_0 = hcB/kT_0$ where B is the appropriate rotational constant for the rigid rotator; b_0 is the spectral line semi-half-width at the pressure p and at the reference temperature T_0 and we have assumed that $b = b_0\sqrt{(T_0/T)}$ at the constant pressure p; $u_0 = h\nu_e/kT_0$ where ν_e represents the normal vibration frequency of the diatomic molecule (harmonic oscillator); E_l = energy of the lower state above the zero-point energy.

From Eqs. (29) and (30) we obtain the following differential equation (after approximating ν in Eq. (29) by ν_0):

$$(\cos\theta')\, ds = \mathscr{A} \frac{b_0}{a_1} \left(\frac{T_0}{T}\right)^{\frac{1}{2}} \frac{\exp(-h\nu_0/kT)}{[1 - \exp(-h\nu_0/kT)]^3} \frac{\exp(E_l/kT)}{[1 - \exp(-u_0 T_0/T)]} \times$$
$$\times \left[1 + \frac{(\nu - \nu_0)^2}{b_0^2(T_0/T)}\right] dT \qquad (31)$$

where

$$\mathscr{A} = \frac{16\pi^2 h^2}{c^4 k} \frac{kT_0}{p} \frac{\nu_0^6}{\sigma_0 T_0^2 g_u A_{u\to l}} \qquad (32)$$

5.1.1. *The limiting case $h\nu_0/kT \ll 1$, $u_0 T_0/T \ll 1$, $(h\nu_0 - E_l)/kT \ll 1$.* For $h\nu_0/kT \ll 1$, $u_0 T_0/T \ll 1$, $(h\nu_0 - E_l)/kT \ll 1$, Eq. (31) becomes, after integration between the limits $s = 0$ at $T = T_0$ and s, T,

$$(\cos\theta')s \simeq \mathscr{A}'(T^{9/2} - T_0^{9/2}) + \mathscr{B}'(T^{11/2} - T_0^{11/2}) \qquad (33)$$

where

$$\mathscr{A}' = \frac{2}{9} \frac{\mathscr{A}(b_0/a_1)}{u_0(h\nu_0/kT_0)^3 T_0^{7/2}}$$
$$\mathscr{B}' = \frac{2}{11} \frac{\mathscr{A}(b_0/a_1)}{u_0(h\nu_0/kT)^3 T_0^{9/2}} \left(\frac{\nu - \nu_0}{b_0}\right)^2 \qquad (34)$$

5.1.2. *The limiting case $h\nu_0/kT \gg 1$, $u_0 T_0/T \gg 1$.* For $h\nu_0/kT \gg 1$, $u_0 T_0/T \gg 1$, and with $z \equiv (h\nu_0 - E_l)/kT$, Eq. (31) becomes

$$(\cos\theta')\, ds \simeq -\mathscr{A} \frac{b_0}{a_1} T_0 \left(\frac{h\nu_0 - E_l}{kT_0}\right)^{\frac{1}{2}} z^{-3/2} e^{-z} \times$$
$$\times \left[1 + \left(\frac{\nu - \nu_0}{b_0}\right)^2 \frac{(h\nu_0 - E_l)}{kT_0} z^{-1}\right] dz \qquad (35)$$

Integrating again from $s = 0$ at $T = T_0$ and $z = z_0 \equiv (h\nu_0 - E_l)/kT_0$ to s, z, we find now that

$$(\cos\theta')\, s \simeq \mathscr{A}\frac{b_0}{a_1} T_0 \left(\frac{h\nu_0 - E_l}{kT_0}\right)^{\frac{1}{2}} I_1 + \mathscr{A} T_0 \frac{b_0}{a_1} \times \left(\frac{h\nu_0 - E_l}{kT_0}\right)^{3/2} \left(\frac{\nu - \nu_0}{b_0}\right)^2 I_2 \tag{36}$$

where
$$I_1 = -\int_{z_0}^{z} z^{-3/2} e^{-z}\, dz, \qquad I_2 = -\int_{z_0}^{z} z^{-5/2} e^{-z}\, dz \tag{37}$$

In order to evaluate I_1 and I_2, it is convenient to write the identity

$$-\int_{z_0}^{z} z^{-n} e^{-z}\, dz = -\int_{\infty}^{z} z^{-n} e^{-z}\, dz + \int_{\infty}^{z_0} z^{-n} e^{-z}\, dz \quad \text{for} \quad n = \frac{3}{2} \text{ or } \frac{5}{2} \tag{38}$$

where the second integral appearing on the right-hand side of Eq. (38) is negligibly small compared to the first for z_0 much larger than z. But

$$-\int_{\infty}^{z} z^{-3/2} e^{-z}\, dz = 2\frac{e^{-z}}{\sqrt{z}} - 2\Gamma(\tfrac{1}{2}) \left\{1 - \frac{\Gamma_z(\frac{1}{2})}{\Gamma(\frac{1}{2})}\right\} \tag{39}$$

where $\Gamma(\frac{1}{2})$ is the complete gamma function of argument $\frac{1}{2}$ and $\Gamma_z(\frac{1}{2})$ is the incomplete gamma function of z of argument $\frac{1}{2}$.[8] Making use of the notation of Pearson,[8] the preceding expression may be rewritten in the form

$$-\int_{\infty}^{z} z^{-3/2} e^{-z}\, dz = 2\left\{\frac{e^{-z}}{\sqrt{z}} - \sqrt{\pi}\left[1 - I\left(\frac{z}{\sqrt{0.5}} - 0.5\right)\right]\right\} \tag{40}$$

With the available tables of the incomplete Γ-function,[8] which give values to seven significant figures, Eq. (40) can only be evaluated for $z < 9$. For $z > 9$, the integrals may be evaluated either numerically or else by using a simple approximation procedure.

Integrating by parts twice yields the expression

$$-\int_{\infty}^{z} z^{-n} e^{-z}\, dz = z^{-n} e^{-z} + \frac{n}{z}\int_{\infty}^{z} z^{-n} e^{-z}\, dz + \int_{\infty}^{z} \frac{n}{z^2}\left(\int_{\infty}^{z} z^{-n} e^{-z}\, dz\right) dz \tag{41}$$

For sufficiently large values of z, Eq. (41) reduces to

$$-\int_{\infty}^{z} z^{-n} e^{-z}\, dz \simeq \frac{z^{-n} e^{-z}}{[1 + (n/z)]} \tag{42}$$

or, in somewhat cruder approximation,

$$-\int_{\infty}^{z} z^{-n} e^{-z}\, dz \simeq z^{-n} e^{-z} \tag{43}$$

Results obtained by using Eqs. (42) and (43), and also by using Eq. (40) together with tabulated values of the incomplete gamma function,[8] are

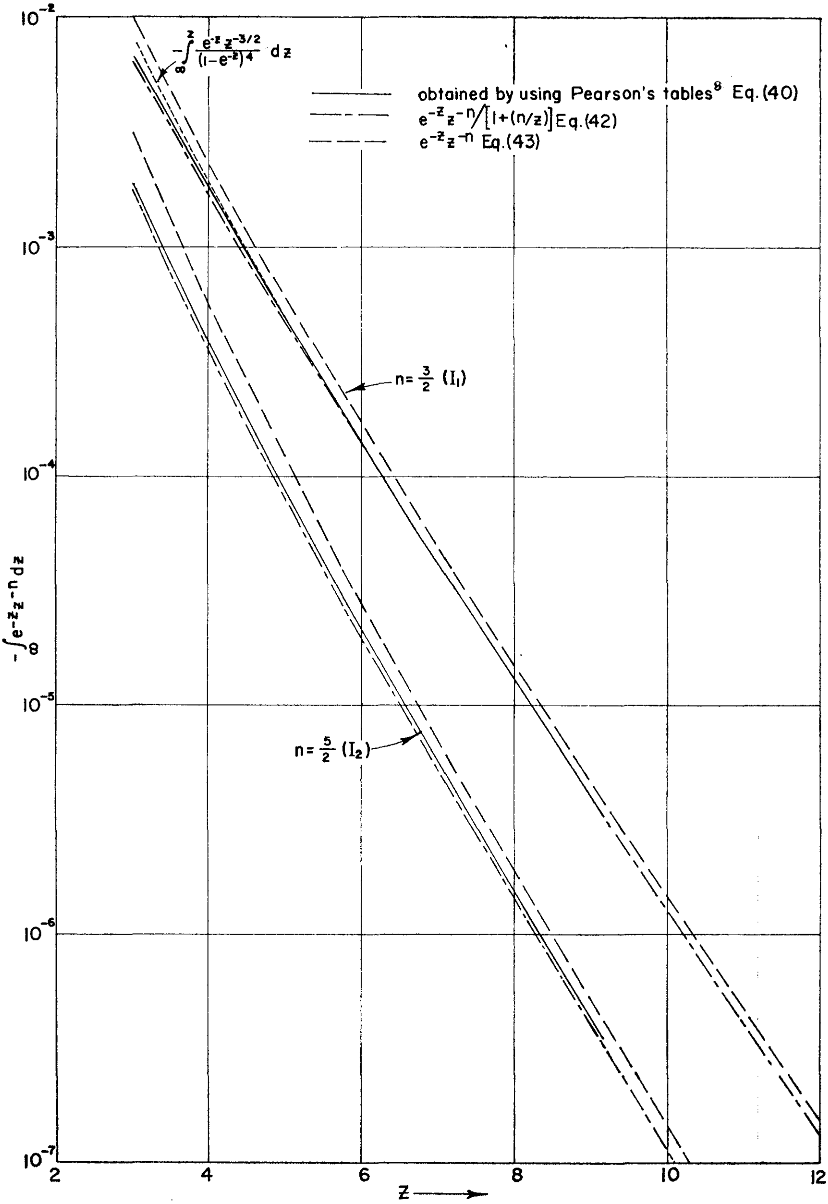

Fig. 4a. The quantity $-\int_{\infty}^{z} e^{-z} z^{-n}\, dz$ *as a function of z for* $3 \leqq z \leqq 12$. *For comparison also*

$$-\int_{\infty}^{z} \frac{e^{-z} z^{-3/2}}{(1 - e^{-z})^4}\, dz$$

is plotted, which determines s(T) for z of the order of 1 *(see Eq.* 31)

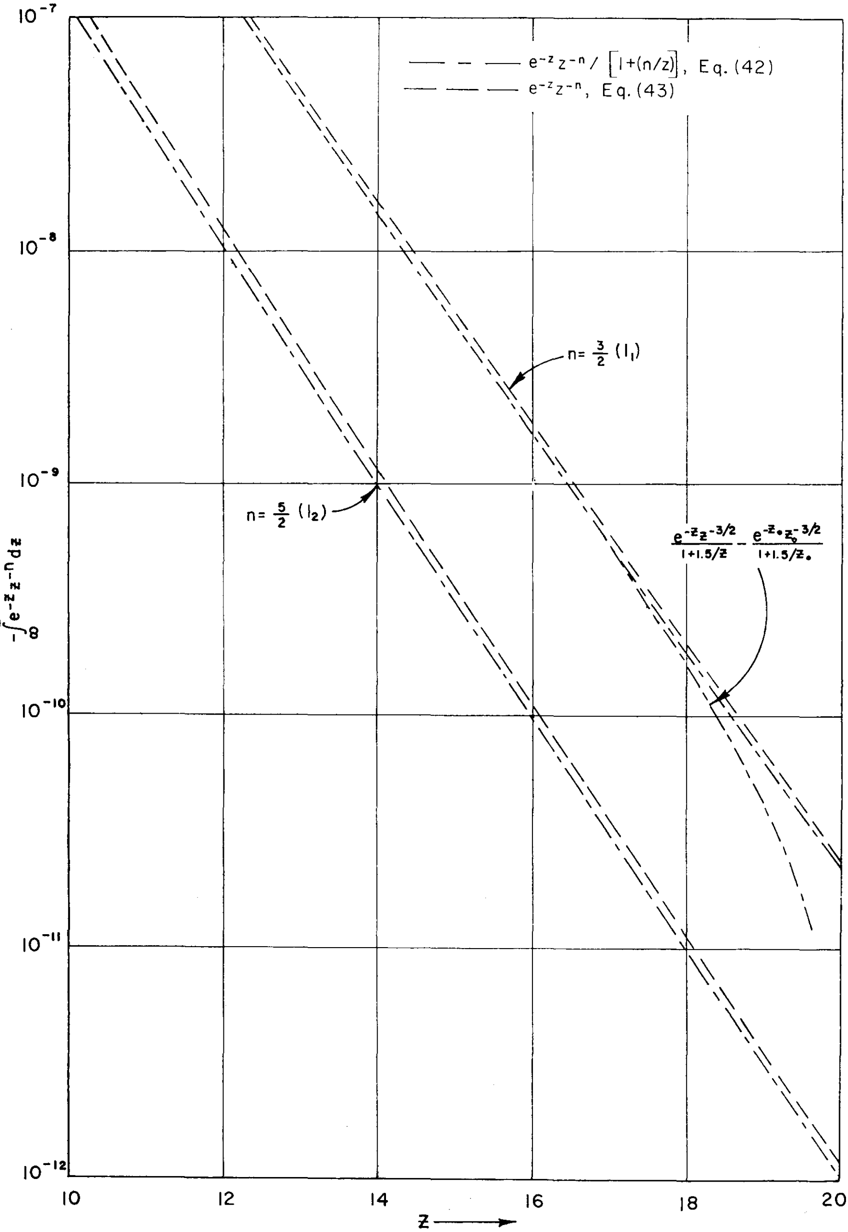

Fig. 4b. The quantity $-\int_{\infty}^{z} e^{-z}z^{-n}\,dz$ *as a function of z for* $10 \leqq z \leqq 20$ $(z_0 = 20)$.

plotted in Figs. 4a and 4b. These data, together with Eqs. (36), (37) and (38) yield the desired temperature profile. For $h\nu_0/kT \ll 1$, the dependence of T on s is easily computed by using Eq. (33).

Reference to Eqs. (33) and (36) shows that the temperature profile depends on the frequency. At the line center, however, $\mathscr{B}' = 0$. Therefore s may be computed as a universal function of T for $h\nu_0/kT_0 \ll 1$. Similarly, for $h\nu_0/kT_0 \gg 1$, the second term in Eq. (36) vanishes and $(\cos\theta') \times \times s/\{\mathscr{A}(b_0/a_1)T_0[(h\nu_0 - E_l)/kT_0]^{\frac{1}{2}}\} = I_1$, which has been plotted in Figs. 4a and 4b for the special cases $z_0 = \infty$ and $z_0 = 20$; in Figs. 5a–5c, the corresponding temperature profiles are shown for $z_0 = 20$, $T_0 = 300°K$.

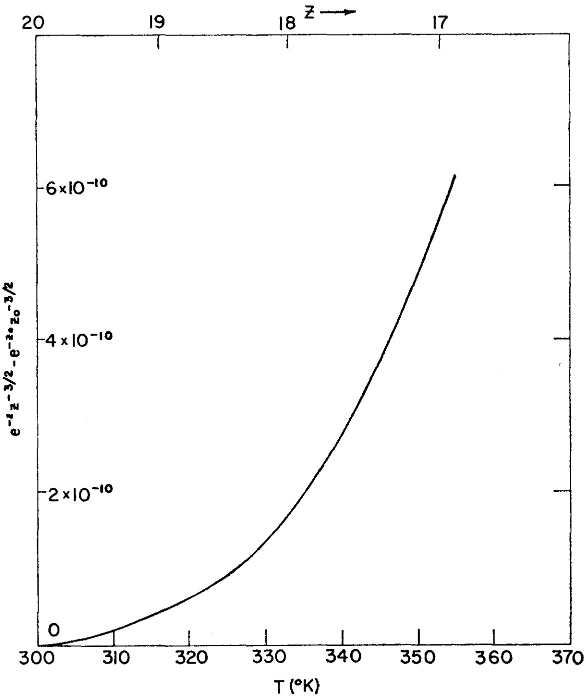

Fig. 5a. A plot of the first approximation to I_1 (see Eq. (43)) as a function of T and z (for $z_0 = 20$, $T_0 = 300°K$, $E_l = 0$).

In the line wings, the first terms of Eqs. (33) and (36) become negligibly small. Hence reduced temperature profiles are again determined in terms of easily computed quantities or in terms of I_2.

5.1.3. *Determination of Steradiancy $B(0, \theta)$ for $h\nu_0/kT_0 \gg 1$, $u_0T_0/T \gg 1$.* If a temperature profile is specified which differs from I_1 or I_2 by at most a constant factor, then the steradiancy $B(0, \theta)$ may be calculated for suitable frequency regions. From Eq. (26) it is apparent that

$$B(0,\theta) = \int_0^\infty B_\nu^0(T_{\tau_\nu = \cos\theta'})\, d\nu \tag{44}$$

where $B_\nu^0(T_{\tau_\nu = \cos\theta'})$ is the blackbody steradiancy at that location where $\tau_\nu/\cos\theta' = 1$. According to Eq. (27),

$$(\cos\theta')a_1 = B_\nu^0(T_{\tau_\nu = \cos\theta'}) - B_\nu^0(T_0) \tag{45}$$

Let us consider the temperature profile $(\cos\theta')s = L_1 I_1$, where the characteristic length L_1 is a constant. Close to the line center, Eqs. (36) and (45) lead to the relation

$$B_\nu^0(T_{\tau_\nu = \cos\theta'}) - B_\nu^0(T_0) = \frac{\mathscr{A}}{L_1} b_0 \left(\frac{h\nu_0 - E_l}{kT_0}\right)^{\frac{1}{2}} T_0(\cos\theta') \tag{46}$$

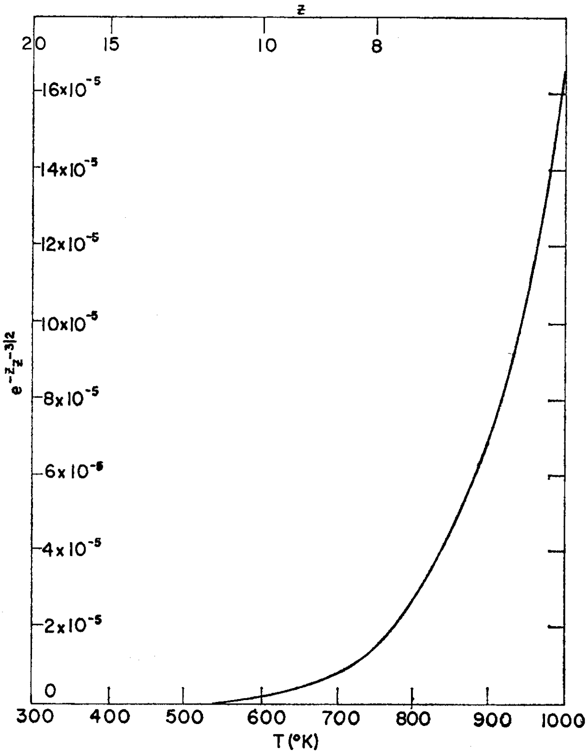

Fig. 5b. A plot of the first approximation to I_1 (see Eq. (43)) as a function of T and z (for $z_0 = 20$, $T_0 = 300°K$, $E_l = 0$). The contribution of the term $e^{-z_0}z_0^{3/2}$ to I_1 is negligibly small.

Next we introduce Eq. (46) into Eq. (44) and integrate from $\nu_0 - \Delta\nu_c$ to $\nu_0 + \Delta\nu_c$, where $\Delta\nu_c$ is sufficiently small to justify use of the first term only in Eq. (36). In this manner we obtain

$$\int_{\nu_0 - \Delta\nu_c}^{\nu_0 + \Delta\nu_c} B_\nu^0(T_{\tau_\nu = \cos\theta'})\, d\nu \simeq 2\left[\frac{\mathscr{A}T_0}{L_1} b_0 \left(\frac{h\nu_0 - E_l}{kT_0}\right)^{\frac{1}{2}}\right] \Delta\nu_c(\cos\theta') \tag{47}$$

where $B_\nu^0(T_0)$ has been neglected.* The contribution of the term in Eq. (38) which has been neglected in Eq. (47), is close to $(\Delta\nu_c/b_0)^2$.

* $B_\nu^0(T_0)$ is negligibly small unless $T \simeq$ const. or $\cos\theta' \simeq 0$.

Let us now consider a temperature profile $(\cos\theta')\,s = L_2 I_2$ and investigate only the contribution of the wings in Eq. (36). Then, proceeding as before,

$$B_\nu^0(T_{\tau_\nu=\cos\theta'}) = \frac{\mathscr{A}}{L_2}\,b_0 T_0\left(\frac{h\nu_0 - E_l}{kT_0}\right)^{3/2}\left(\frac{\nu-\nu_0}{b_0}\right)^2(\cos\theta') + B_\nu^0(T_0) \tag{48}$$

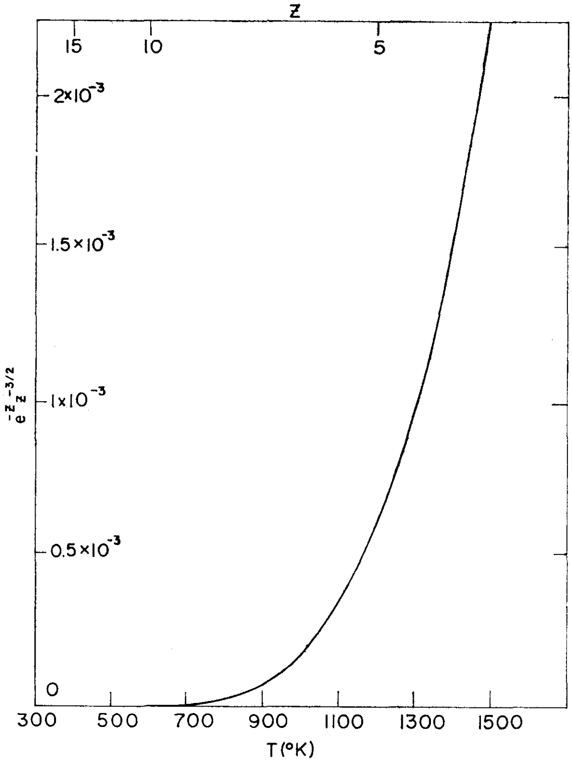

Fig. 5c. A plot of the first approximation to I_1 (see Eq. (43)) as a function of T and z (for $z_0 = 20$, $T_0 = 300°K$, $E_l = 0$). The contribution of the term $e^{-z_0}z_0^{3/2}$ to I_1 is negligibly small.

Introducing Eq. (48) into Eq. (44), we obtain the following integral

$$2\int_{\nu_0+\Delta\nu_w}^{\nu_0+\Delta\nu_w^u} B_\nu^0(T_{\tau_\nu=\cos\theta'})\,d\nu$$

$$= \frac{2\mathscr{A}}{L_2}\,b_0^2\,T_0\left(\frac{h\nu_0 - E_l}{kT_0}\right)^{3/2}\cos\theta'\int_{\Delta\nu_w/b_0}^{\Delta\nu_w^u/b_0}\left(\frac{\nu-\nu_0}{b_0}\right)^2 d\left(\frac{\nu-\nu_0}{b_0}\right) \tag{49}$$

where $B_\nu^0(T_0)$ has been neglected. The integration limit towards the line center, $\nu_0 + \Delta\nu_w$, must be chosen sufficiently large so that the first term in Eq. (36) is negligibly small. The upper limit, $\nu_0 + \Delta\nu_w^u$, must be consistent with the restriction that $\tau_\nu = \cos\theta'$ for all ν. Clearly the basic relation given in Eq. (26) can only hold provided $T_{\tau_\nu = \cos\theta'} \leqq T_{\max}$, where $T_{\max}$ is the highest temperature of the system, i.e. the value of $\Delta\nu_w^u$ is determined by the expression

$$\frac{\Delta\nu_w^u}{b_0} \simeq \left[\frac{B_\nu(T_{\max})L_2}{\mathscr{A} b_0 T_0 (\cos\theta')}\left(\frac{kT_0}{h\nu_0 - E_l}\right)^{3/2}\right]^{\frac{1}{2}} \tag{50}$$

Hence Eq. (49) becomes

$$2\int_{\nu_0+\Delta\nu_w}^{\nu_0+\Delta\nu_w^u} B_\nu^0(T_{\tau_\nu = \cos\theta'})\,d\nu \simeq \frac{2}{3}\frac{\mathscr{A}}{L_2} b_0^2 T_0 \left(\frac{h\nu_0 - E_l}{T_0}\right)^{3/2} (\cos\theta') \times$$

$$\times \left\{\left[\frac{B_\nu^0(T_{\max})L_2}{\mathscr{A} T_0 b_0 (\cos\theta')}\left(\frac{kT_0}{h\nu_0 - E_l}\right)^{3/2}\right]^{3/2} - \left(\frac{\Delta\nu_w}{b_0}\right)^3\right\} \tag{51}$$

From Eqs. (47) and (51) we may now determine the scaling parameters for the steradiancy. Since $\Delta\nu_c \propto b_0$ for a fixed ratio of the second term (which has been neglected) relative to the first term in Eq. (36), we find

$$\int_{\nu_0-\Delta\nu_c}^{\nu_0+\Delta\nu_c} B_\nu^0(T_{\tau_\nu = \cos\theta'})\,d\nu \propto \frac{\rho_0}{L_1} \tag{52}$$

and

$$2\int_{\nu_0+\Delta\nu_w}^{\nu_0+\Delta\nu_w^u} B_\nu^0(T_{\tau_\nu = \cos\theta'})\,d\nu \propto \rho_0\sqrt{L_2} \text{ for } \Delta\nu_w \ll \Delta\nu_w^u \tag{53}$$

The result given in Eq. (53) is identical with the scaling parameter obtained for the wings of isothermal collision-broadened lines. This conclusion is consistent with Thomson's approximate considerations.[9]

5.2. *Isolated Spectral Lines Belonging to Diatomic Emitters with Doppler Broadening*

For Doppler-broadened lines, we find

$$k_\nu = \frac{c^2}{8\pi\nu_0^2} A_{u\to l}\, g_u \left(\frac{p}{kT_0}\right)\frac{\sigma_0}{b_{D,0}}\left(\frac{\ln 2}{\pi}\right)^{\frac{1}{2}}\left(\frac{T_0}{T}\right)^{5/2}[1 - \exp(-u_0 T_0/T)] \times$$

$$\times [1 - \exp(-h\nu_0/kT)][\exp(-E_l/kT)] \exp\left[-(\ln 2)\left(\frac{\nu - \nu_0}{b_{D,0}}\right)^2 \frac{T_0}{T}\right] \tag{54}$$

where the Doppler half-width under reference conditions is given by

$$b_{D,0} = \left(\frac{2kT_0 \ln 2}{mc^2}\right)^{\frac{1}{2}} \nu_0$$

From Eqs. (29) and (54) we find that

$$ds = \frac{\mathscr{A} b_{D,0}}{a_1 (\cos\theta')} \left(\frac{1}{\pi \ln 2}\right)^{\frac{1}{2}} \left(\frac{T}{T_0}\right)^{\frac{1}{2}} \frac{\exp\ (-h\nu_0/kT)}{[1-\exp(-h\nu_0/kT]^3} \frac{\exp\ (E_l/kT)}{[1-\exp(-u_0 T_0/T)]} \times$$

$$\times \exp\left[(\ln 2)\left(\frac{\nu-\nu_0}{b_{D,0}}\right)^2 \frac{T_0}{T}\right] dT \qquad (55)$$

where $\mathscr{A}$ is given by Eq. (32).

5.2.1. *The limiting case* $h\nu_0/kT \ll 1$, $u_0 T_0/T \ll 1$, $(h\nu_0 - E_l)/kT \ll 1$. Equation (55) becomes now

$$(\cos\theta')\, ds \cong \frac{\mathscr{A} b_{D,0}}{a_1 u_0}\left(\frac{kT_0}{h\nu_0}\right)^3 \left(\frac{1}{\pi \ln 2}\right)^{\frac{1}{2}} \left(\frac{T}{T_0}\right)^{9/2} \exp\left[(\ln 2)\left(\frac{\nu-\nu_0}{b_{D,0}}\right)^2 \frac{T_0}{T}\right] dT \qquad (56)$$

We define the region near the line center by the condition that the exponential term may be replaced by unity. In this case

$$(\cos\theta')s = \mathscr{A}''[(T/T_0)^{11/2} - 1] \qquad (57)$$

where

$$\mathscr{A}'' = \frac{2}{11} \frac{\mathscr{A} b_{D,0} T_0}{u_0 a_1}\left(\frac{1}{\pi \ln 2}\right)^{\frac{1}{2}} \left(\frac{kT_0}{h\nu_0}\right)^3$$

When the exponent is sufficiently large, the following approximation may be used:

$$(\cos\theta')s = \mathscr{B}''\left\{\exp\left[(\ln 2)\left(\frac{\nu-\nu_0}{b_{D,0}}\right)^2\right] - \left(\frac{T}{T_0}\right)^{13/2} \exp\left[(\ln 2)\left(\frac{\nu-\nu_0}{b_{D,0}}\right)^2 \left(\frac{T_0}{T}\right)\right]\right\} \qquad (58)$$

where

$$\mathscr{B}'' = \frac{\mathscr{A} b_{D,0}}{u_0 a_1 \ln 2} T_0 \left(\frac{1}{\pi \ln 2}\right)^{\frac{1}{2}} \left(\frac{kT_0}{h\nu_0}\right)^3 \left(\frac{b_{D,0}}{\nu-\nu_0}\right)^2$$

5.2.2. *The limiting case* $h\nu_0/kT \gg 1$, $u_0 T_0/T \gg 1$. Integration of Eq. (55) yields the expression

$$s = \frac{\mathscr{A} b_{D,0} T_0}{a_1(\cos\theta')}\left(\frac{1}{\pi \ln 2}\right)^{\frac{1}{2}} \left[\frac{h\nu_0}{kT_0} - \frac{E_l}{kT_0} - (\ln 2)\left(\frac{\nu-\nu_0}{b_{D,0}}\right)^2\right]^{3/2} \times$$

$$\times \left[-\int_{w_0}^{w} w^{-5/2} e^{-w}\, dw\right] \qquad (59)$$

where

$$w = \left[\frac{h\nu_0}{kT_0} - \frac{E_l}{kT_0} - (\ln 2)\left(\frac{\nu-\nu_0}{b_{D,0}}\right)^2\right]\frac{T_0}{T}$$

For $w > 0$, we may proceed as with the collision-broadened line and the integral

$$I_2' = -\int_{w_0}^{w} w^{-5/2} e^{-w}\, dw \tag{60}$$

may be evaluated by using the methods of Section 5.1.2.

Having assumed $h\nu_0/kT_0 \gg 1$, the frequency region for $w < 0$ occurs far out in the line wings and contributes relatively little to the total steradiancy.

5.2.3. *Determination of steradiancy* $B(0, \theta)$ *for* $h\nu_0/kT \gg 1$, $u_0T_0/T \gg 1$, $(h\nu_0 - E_l)/kT \gg 1$. The frequency dependence of ds/dT given in Eq. (59) does not permit us to choose $a_1(\nu)$ in such a way that a reduced distance–temperature profile can be constructed. The difficulty is caused by the occurrence of a product of frequency- and temperature-dependent terms in the exponent.

Near the line center, we may, however, calculate the radiant flux since the integral I_2' is determined almost entirely by its upper limit $w_{\min}$ (corresponding to $T = T_{\max}$) provided that $w_0 - w_{\min} \gtrsim 2$. This property of the integral has been discussed in Section 5.1.2. Introducing the additional restrictions

$$\left.\begin{aligned} &\left(\frac{\nu - \nu_0}{b_{D,0}}\right)^2 \ln 2 \ll \frac{h\nu_0 - E_l}{kT_0} \\ \text{and}\quad &\\ &\left(\frac{\nu - \nu_0}{b_{D,0}}\right)^2 (\ln 2)\, \frac{T_0}{T_{\max}} \ll 1 \end{aligned}\right\} \tag{61}$$

Eq. (59) becomes

$$s \simeq \frac{\mathscr{A} b_{D,0} T_0}{a_1(\cos\theta')} \left(\frac{1}{\pi \ln 2}\right)^{\frac{1}{2}} \left(\frac{h\nu_0 - E_l}{kT_0}\right)^{3/2} I_2'' \tag{62}$$

where

$$I_2'' = -\int_{\infty}^{z} z^{-5/2} e^{-z}\, dz, \quad z = (h\nu_0 - E_l)/kT$$

and z is independent of ν.

The inequalities in Eq. (61) become, for typical fundamental vibration-rotation bands of diatomic molecules,

$$\left(\frac{\nu - \nu_0}{b_{D\,0}}\right)^2 \ll 30$$

and

$$\left(\frac{\nu - \nu_0}{b_{D,0}}\right)^2 \ll 1.4\, \frac{T_{\max}}{T_0}$$

Hence, for large values of $T_{\max}/T_0$, the correct integral is obtained for a frequency range that may be appreciably larger than $b_{D,0}$. On the other hand, for systems with small temperature gradients, we have obtained a temperature profile that is applicable only very close to the line center.

For the temperature profile $s(\cos\theta') = L_3 I_2$, we find, after integrating over the frequency range from $\nu_0 - \Delta\nu_D$ to $\nu_0 + \Delta\nu_D$ (compare Eq. (47)), that

$$\int_{\nu_0-\Delta\nu_D}^{\nu_0+\Delta\nu_D} B_\nu(T_{\tau_\nu=\cos\theta'})\,d\nu = 2\left[\frac{\mathscr{A} b_{D,0} T_0}{L_3}\left(\frac{1}{\pi\ln 2}\right)^{\frac{1}{2}} \times \right.$$
$$\left. \times \left(\frac{h\nu_0 - E_l}{kT_0}\right)^{3/2}(\cos\theta')\right]\Delta\nu_D \tag{63}$$

In general, the integral represents only the contributions arising from a narrow frequency range near the line center. Since it is reasonable to assume that $\Delta\nu_D$ is proportional to $b_{D,0}$, the radiancy for this frequency range near the line center is inversely proportional to $\rho_0 L_3$.

5.3. *Gray Body*

With

$$k_\nu(T) = \bar{k} = \text{const}$$

integration of Eq. (29) leads to the expression

$$s(\cos\theta') = \frac{1}{a_1\bar{k}}\frac{2h\nu^3}{c^2}\left[\frac{1}{\exp(h\nu/kT)-1} - \frac{1}{\exp(h\nu/kT_0)-1}\right] \tag{64}$$

In important regions of frequency and temperature, Eq. (64) reduces to a universal relation between s and T.

5.3.1. *The special case $h\nu/kT < h\nu/kT_0 \ll 1$*

Equation (64) now reduces to

$$s(\cos\theta') = \frac{2k\nu^2}{a_1\bar{k}c^2}(T - T_0) \tag{65}$$

Hence, for

$$s(\cos\theta') = \bar{L}(T - T_0) \tag{66}$$

Eqs. (44) and (45) lead to

$$\int_{\nu_1}^{\nu_2} B_\nu(0,\theta)\,d\nu = \int_{\nu_1}^{\nu_2} B_\nu^0(T_0)\,d\nu + \frac{2k}{3\bar{L}\bar{k}c^2}(\nu_2^3 - \nu_1^3)(\cos\theta') \tag{67}$$

and, if $T \gg T_0$, then

$$\int_{\nu_1}^{\nu_2} B_\nu(0,\theta)\,d\nu \propto (\rho_0\bar{L})^{-1};$$

the scaling parameter is $\rho_0\bar{L}$.

5.3.2. *The special case $h\nu/kT_0 \gg 1$, $h\nu/kT \ll 1$*

In Eq. (65), T replaces $(T - T_0)$ and the preceding results apply.

5.3.3. *The special case $h\nu/kT_0 \gg 1$, $h\nu/kT \gg 1$*

In this case there is no $s - T$ curve which is independent of ν.

6. RADIATIVE SCALING PROPERTIES FOR REPRESENTATIVE TEMPERATURE PROFILES

The integral expression of Section 1.3 for the spectral steradiancy B_ν is the formal solution to the linear, first-order differential equation

$$\frac{dB_\nu}{ds^*} = L_0 k_\nu (B_\nu^0 - B_\nu) \tag{68}$$

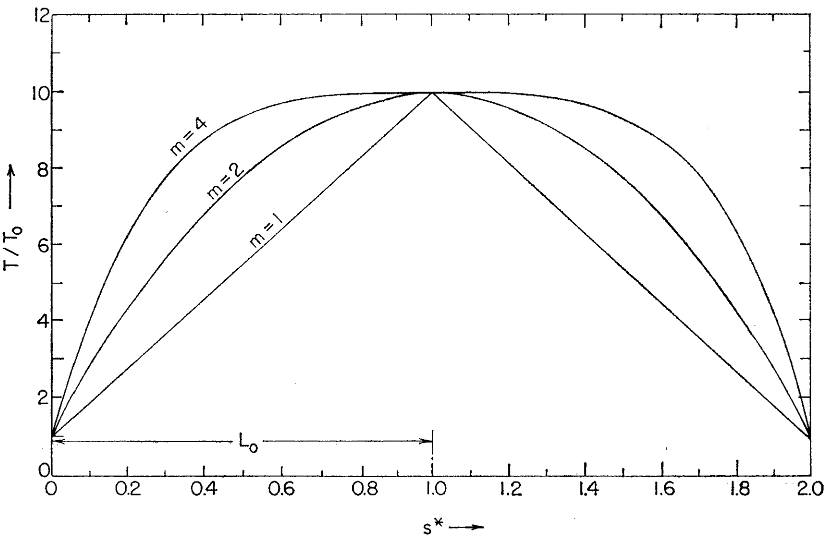

Fig. 6. Representative temperature profiles described by Eq. (69) *for* $m = 1, 2$ *and* 4.

where $s^* = s/L_0$, s is the distance along the line of sight, and L_0 is a characteristic length of the system. Equation (68) has been integrated numerically by means of a fourth order Runga–Kutta method for representative temperature profiles. The temperature profiles are represented by the expressions

$$T = (T_{\max} - T_0)(1 - |\, s^* - 1 \,|^m) + T_0, \quad m = 1, 2, 4 \tag{69}$$

The specified temperature profiles are sketched in Fig. 6.

The absorption coefficient k_ν is given by Eqs. (30) and (54) for dispersion- and Doppler-broadened line contours, respectively. The spectral and total line steradiancies at $s^* = 2$ have been computed for a typical strong line of the vibration-rotation spectrum of the hydrogen fluoride molecule. We have chosen the values $T_0 = 300°\text{K}$ and $T_{\max} = 3000°\text{K}$. Representative results of the calculations are shown in Figs. 7, 8, and 9 for the $R3(v = 0, J = 3 \rightarrow v = 1, J = 4)$ line of HF. For this line in case of dispersion-broadening, $b_0/c = 0.132p$ cm^{-1}(p in atm) whereas for Doppler broadening

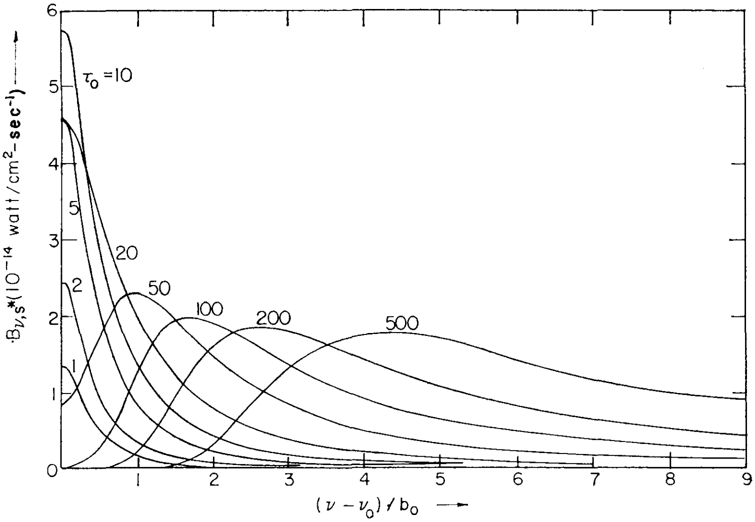

Fig. 7. *The spectral steradiancies* B_{ν,s^*} *for* $m = 2$ *for the R3 line of* HF *at* $s^* = 2$ *as a function of* $(\nu - \nu_0)/b_0$ *for pure dispersion-broadening and various values of the reference optical depth* τ_0.

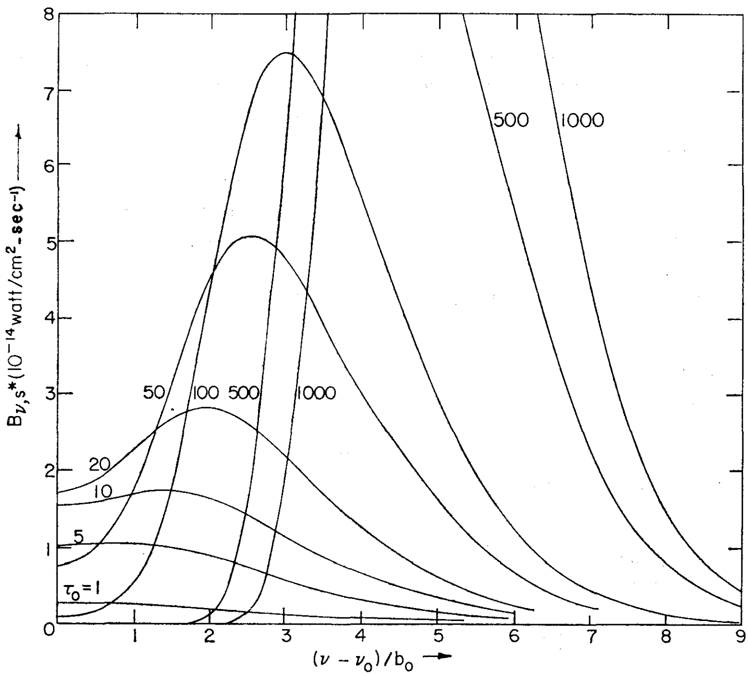

Fig. 8. *The spectral steradiancies* B_{ν,s^*} *for* $m = 2$ *for the R3 line of* HF *at* $s^* = 2$ *as a function of* $(\nu - \nu_0)/b_0$ *for pure Doppler broadening and various values of the reference optical depth* τ_0.

we have used $b_0/c = 5.85 \times 10^{-3}\,\text{cm}^{-1}$. The reference optical depth is defined as $\tau_0 = (L_0/\pi b_0) \int k_{\nu,0} d\nu (k_{\nu,0} =$ absorption coefficient evaluated at the frequency ν at T_0), B_{ν,s^*} is the spectral steradiancy at $s^* = 2$, and B_{s^*} represents the integrated steradiancy at $s^* = 2$ for the entire line.

Reference to Fig. 9 shows that Doppler and dispersion-broadening produce the same total steradiancy B_{s^*} for the case under consideration for large values of τ_0 provided that $b_{0,\,\text{dispersion}} \simeq 2b_{0,\,\text{Doppler}}$, i.e. for $p \simeq 0.1$ atm.

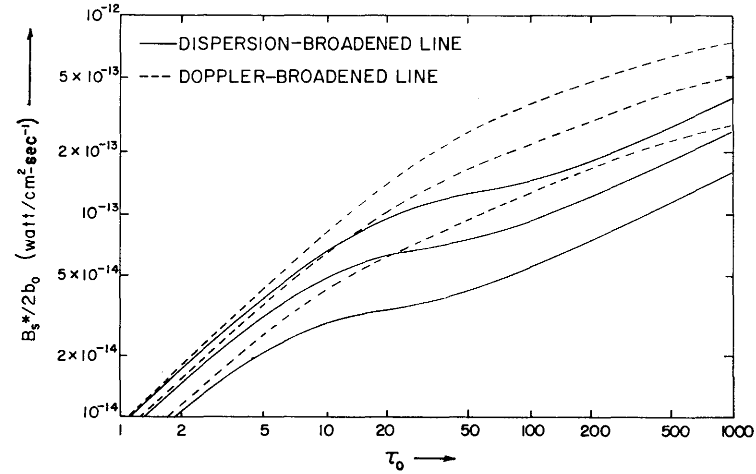

Fig. 9. The total steradiancy divided by $2b_0$ $(\equiv B_{s^*}/2b_0)$ *at* $s^* = 2$ *as a function of* τ_0 *for the dispersion- and Doppler-broadened* R3 *line of* HF, $T_0 = 300°K$, $T_{\text{max}} = 3000°K$, *for various values of m in Eq.* (69).

6.1. *Dispersion-Broadened Line*

Examination of Fig. 7 shows that the R3 line of HF retains a typical dispersion contour until τ_0 becomes greater than about 10, when self-reversal becomes important. Hence $\tau_0 \simeq 10$ may be said to define the upper limit of the transparent gas regime. From Fig. 9 it is seen that the pressure and length dependence of the steradiancy for $\tau_0 \gtrsim 10$ is

$$B_{s^*} \propto \rho_0 L_0 \tag{70}$$

i.e. it is the same as for an isothermal transparent gas. In general, $\tau_0 = 10$ corresponds to a small physical length for a strong spectral line. For the R3 line of HF, the value of L_0 at $\tau_0 = 10$ is about 0.015 cm.

The center of the line is essentially completely self-absorbed fo r$\tau_0 \simeq 100$.* Figure 9 shows that for $\tau_0 \gtrsim 100$

$$B_{s^*} \propto \sqrt{(\rho_0^2 L_0)} \tag{71}$$

which is the same as for the Eddington–Barbier approximation or for the isothermal case for large optical depths. For a strong line, the transition to the regime described by Eq. (71) occurs at a small physical length ($\simeq 0.15$ cm for the R3 line of HF).

* The condition that the steradiancy is proportional to $(\rho^2 L_0)^{1/2}$, for values of τ_0 exceeding the value required to make the line center "black", may be used for the derivation of an approximate relation for the critical minimum value of τ_0 above which Eq. (71) applies for various temperature profiles (for details, see the Ph. D. thesis of M. Thomas, California Institute of Technology, Pasadena, June 1964).

6.2. *Doppler-Broadened Line*

The plot in Fig. 8 shows that self-reversal for the Doppler-broadened line becomes important for $\tau_0 \simeq 5$. However, reference to Fig. 9 indicates that Eq. (70) remains valid up to $\tau_0 \simeq 10$ which, at $p = 0.1$ atm, corresponds to $L_0 \simeq 0.007$ cm for the R3 line of HF. For larger values of τ_0, however, the Doppler-broadened line does not approximate the behavior of the dispersion-broadened line, i.e. B does not become simply proportional to a power of L_0. Rather, B_{s*} becomes a weaker and weaker function of τ_0 as saturation is approached.

The more complicated behavior of the Doppler-broadened line compared to the dispersion-broadened line is the result of the fact that the Doppler line half-width increases with temperature while the dispersion line half-width decreases with temperature at constant pressure. Hence, viewing a Doppler-broadened system at $s^* = 2$, the radiation emitted from the higher temperature regions is " seen " at all optical depths since this radiation is not extensively reabsorbed.

7. CONCLUDING REMARKS

The development presented in Sections 5 and 6 indicates that a similarity analysis utilizing isothermal approximations for the radiative energy transport constitutes an acceptable approximation for dispersion-broadened lines for a variety of important temperature profiles. On the other hand, excepting only the transparent gas regime, it is not possible to represent a non-isothermal radiating system with Doppler-broadened lines by an equivalent isothermal distribution. Hence simplified procedures for studying the interplay between flow, chemical reactions, and radiative energy transport can generally be employed only for non-isothermal emitters with dispersion lines.

REFERENCES

1. Penner, S. S., *Combustion Researches and Reviews, 1955*, pp. 140–162, Butterworths Scientific Publications, London 1956.
2. Nachbar, W., Williams, F. A. and Penner, S. S., Quart. Appl. Math. **17**, 43, 1959.
3. Penner, S. S., *Chemistry Problems in Jet Propulsion*, Pergamon Press, London 1957.
4. Hirschfelder, J. O., University of Wisconsin Report WIS–ONR–18, February 6, 1956; Butler, J. N. and Brokaw, R. S., *J. Chem. Phys.* **26**, 1636, 1957.
5. Hirschfelder, J. O., Curtiss, C. F. and Bird, R. B., *Molecular Theory of Gases and Liquids*, Wiley, New York 1954.
6. Penner, S. S. and Patch, R. W., " Radiative Transfer Studies and Opacity Calculations for Heated Gases ", Technical Report No. 6, Contract AF 49 (638)–984, California Institute of Technology, Pasadena, Calif., January 1962; in press in *Papers Presented in Honor of Modesto Panetti*, Politecnico di Torino, Torino, Italy, 1962.
7. Unsöld, A., *Physik der Sternatmosphären*, Julius Springer, Berlin 1958.
8. Pearson, K., *Tables of the Incomplete Γ-Function*, Cambridge University Press, Cambridge 1957.
9. Thomson, J. A. L., *Eighth International Combustion Symposium*, pp. 69–81, Williams and Wilkins, Baltimore 1962.